

一种低暗计数率P-I-N结构的单光子雪崩二极管探测器

李峰¹, 刘丹璐¹, 董杰¹, 卞大井¹, 徐跃^{1,2*}¹南京邮电大学集成电路科学与工程学院, 江苏 南京 210023;²射频集成与微组装技术国家地方联合实验室, 江苏 南京 210023

摘要 基于180 nm BCD工艺制备出一种P型注入增强型P-I-N结构的单光子雪崩二极管(SPAD)探测器。采用P型漂移区与高压N⁺埋层之间的低掺杂浓度P型外延层作为I层深结雪崩区,提高了近红外波段的光子探测概率(PDP)。利用低掺杂浓度的P型外延层作为虚拟保护环,防止了器件横向击穿,降低了暗计数率(DCR)。测试结果表明,虚拟保护环宽度(GRW)为5 μm时,器件雪崩电压为56 V。在5 V过偏压下600 nm处的峰值PDP为41%,在901 nm的近红外波段下PDP大于6%,DCR为0.56 s⁻¹·μm⁻²,后脉冲率小于1.2%,表现出良好的电学和光学特性。所提出的SPAD器件为硅基高灵敏度近红外单光子探测器设计提供了一种可选的解决方案。

关键词 探测器; 单光子雪崩二极管(SPAD); P-I-N结构; 光子探测概率(PDP); 暗计数率(DCR)

中图分类号 TN491

文献标志码 A

DOI: 10.3788/AOS231800

1 引言

硅基单光子雪崩二极管(SPAD)探测器具有低成本、高灵敏度、皮秒级响应速度、低噪声等优点,它可以与后端电路集成在同一芯片衬底上,构成高密度成像传感器。SPAD探测器在量子通信、激光雷达、荧光寿命成像等光学传感领域具有良好的应用前景^[1-2]。激光雷达和3D成像系统不仅要求硅基SPAD探测器具有高集成度和小型化的特点,还要求其能工作在近红外波段内,满足脉冲激光发射波长对人眼安全的要求。然而,硅基SPAD器件对近红外光子的探测能力很弱,因此需要研究新的SPAD器件结构来提高近红外波段的光子探测概率(PDP)。

近年来,研究人员采用低成本互补金属氧化物半导体(CMOS)工艺设计出多种器件结构来提高SPAD对近红外波段的PDP。传统的P⁺/N阱和P阱/深N阱(DNW)等浅结SPAD结构^[3]的雪崩倍增区靠近器件表面,近红外光谱响应度较低,而且受高密度陷阱的浅沟隔离(STI)影响较大,器件暗计数率(DCR)较高,这就限制了单光子探测能力。采用背照式P⁺/DNW或P⁺/N阱结构^[3-4]的SPAD具有高的量子效率,在较低过偏压下就能实现高的PDP,但高昂的制造成本限制了它们的普及^[5]。近几年,科研人员又提出了P-I-N结构SPAD^[2,6],其特点是具有较深且宽的雪崩倍增区,可承受更高的过偏压(V_{ex}),从而提高了近红

外波段的PDP。目前,采用低成本硅基工艺提高近红外波段的PDP正成为SPAD器件的研究重点。

本文从优化近红外波段的PDP和DCR的角度出发,基于180 nm BCD (Bipolar-CMOS-DMOS)工艺提出一种P型注入增强型P-I-N结构的SPAD器件。与现有P-I-N结构相比,该结构SPAD具有更强的深雪崩电场,提高了对近红外光子的探测能力。通过在深结的P型漂移区内增加额外的P型注入区,增强了雪崩倍增区电场,获得了宽光谱响应范围,提高了近红外波段的PDP;采用低掺杂浓度的P型外延层作为虚拟保护环,避免了提前击穿,减小了DCR;采用高压N⁺埋层实现与P型衬底隔离,防止了串扰。测试结果表明,该器件在 $V_{ex}=5$ V时901 nm处的PDP超过6%,DCR仅为0.56 s⁻¹·μm⁻²。

2 器件结构设计与仿真

基于180 nm BCD工艺设计了一种P型注入增强型P-I-N结构的SPAD器件,其截面如图1所示。器件的深雪崩倍增区位于P型漂移区(PDRF)和高压N⁺埋层(HVBN)之间,具有较大的耗尽层宽度,特别是在PDRF层里增加一个额外的P型注入层,增强了雪崩电场,有利于近红外光子触发雪崩效应,从而提高SPAD对近红外光子的响应度。同时,通过优化保护环设计来降低器件的暗噪声。在P⁺阳极区域周围设置低压P阱(PW)保护环,同时利用轻掺杂P型外延层

收稿日期: 2023-11-16; 修回日期: 2024-02-05; 录用日期: 2024-02-27; 网络首发日期: 2024-03-13

基金项目: 国家自然科学基金(62171233)、核探测与核电子学国家重点实验室资助项目(SKLPDE-KF-202307)

通信作者: *yue@njupt.edu.cn

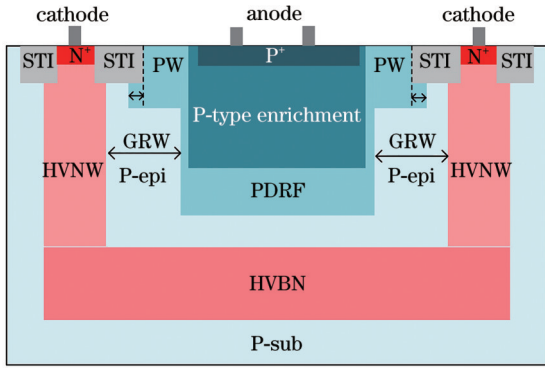


图1 P-I-N结构SPAD的截面图

Fig. 1 Cross-sectional view of P-I-N SPAD

作为一个深的虚拟保护环,从而避免了雪崩区的边缘击穿(PEB)。此外,在器件表面设有浅沟槽隔离(STI),将阳极和阴极隔离并防止在表面上形成电场。该双保护环的设计使器件的有源区远离STI区域,有效避免了STI区域大量缺陷通过漂移进入雪崩倍增区而触发暗计数,从而使SPAD获得低的暗计数噪声^[7]。高压N阱(HVNW)用作HVBN的拾取层,与阴极连接。高压N⁺埋层(HVBN)实现雪崩倍增区与衬底隔离^[8],可避免由光学串扰引起的雪崩事件,而且HVBN还能减小器件的串联电阻,降

低击穿电压。

为了验证上述结构的可行性,使用Silvaco TCAD软件进行TCAD器件仿真。使用与杂质浓度相关的Conmob和低场的Fldmob迁移率模型、SRH复合模型、Selberherr碰撞电离模型、Band-to-band tunneling(BTBT)隧穿模型和Geiger模型,提取雪崩电压、电场、电流等重要器件参数。定义器件的电极、区域与掺杂,器件阴极之间的距离为18 μm,有源区直径为7 μm。考虑到保护环宽度(GRW)过小会导致器件表面提前击穿,而GRW过大会降低填充因子和光子探测效率(PDE),为了保证SPAD器件填充因子并且避免PEB,设置GRW分别为3、4、5 μm(对应于D₁、D₂、D₃)的器件,根据仿真结果选出最优结构并进行流片测试。

对新型P-I-N结构SPAD的I-V特性进行仿真,3种结构SPAD器件的I-V特性如图2(a)所示。当GRW为3 μm时,器件在表面P阱保护环内发生提前击穿;图2(b)展示了电场随器件剖面深度变化的仿真结果,强电场均匀分布在雪崩倍增区,GRW为4 μm或5 μm时峰值电场约为3.29×10⁵ V/cm,相比GRW为3 μm时有较大提升。当GRW为4 μm时,器件正常雪崩,但是保护环区域的电场较强,会恶化暗计数噪

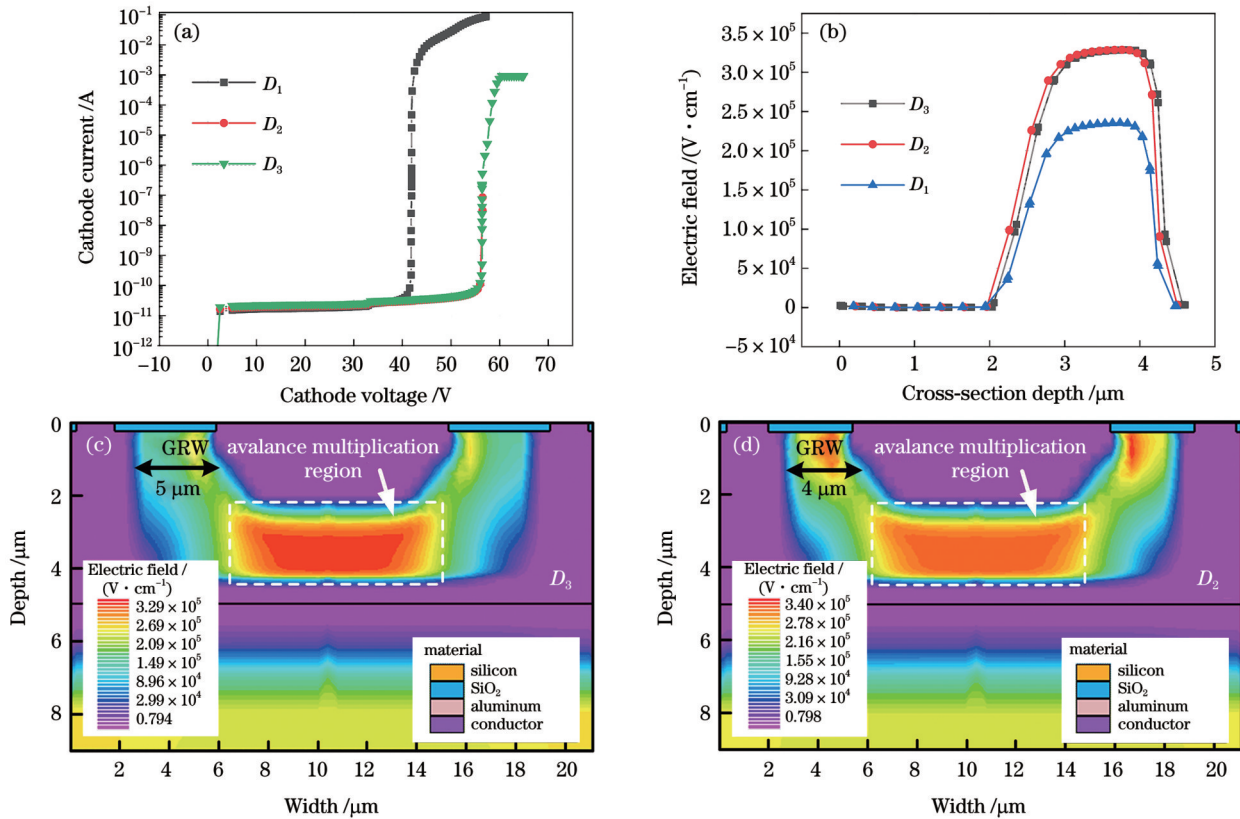


图2 SPAD器件仿真结果。(a) P-I-N结构SPAD器件的I-V特性曲线;(b) P-I-N结构SPAD器件的电场分布;(c)二维电场分布(D₃);(d)二维电场分布(D₂)

Fig. 2 Simulation results of SPAD. (a) I-V curves of P-I-N SPAD; (b) electric field distribution of P-I-N SPAD; (c) 2D electric field distribution (D₃); (d) 2D electric field distribution (D₂)

声[图 2(c)];当 GRW 为 5 μm 时,器件的雪崩电压为 56 V,雪崩倍增区电场最强,且均匀分布,而 P 阱保护环的电场很弱,符合设计需求。

3 测试结果与讨论

3.1 I-V 特性

图 3(a)为 SPAD 器件的显微照片,使用半导体

参数分析仪(Keithley 4200A)测试 $D_3=5 \mu\text{m}$ 时的 I-V 特性,图 3(b)所示为暗环境下 SPAD 的雪崩电压和暗电流。雪崩电压约为 56 V,与仿真结果较为接近。无光照时器件暗电流为 pA 量级,当反向偏压增加至雪崩电压时,暗电流迅速上升,与仿真结果一致。光照环境下,电流增大了约 4 个数量级,器件能够正常工作。

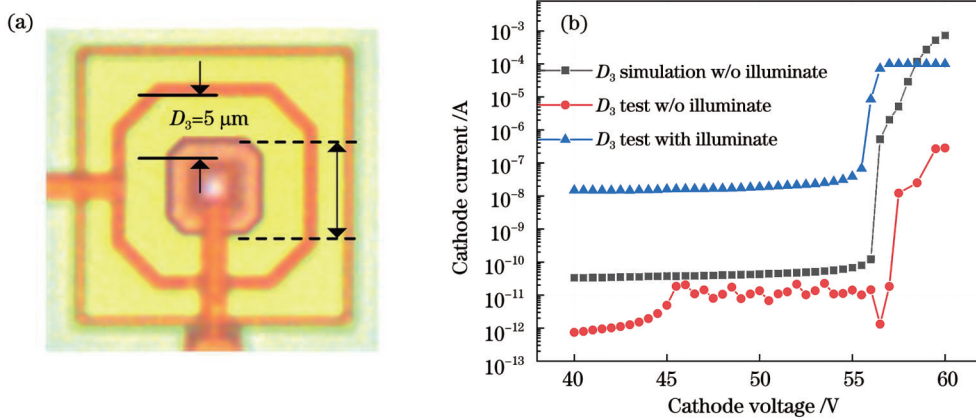


图 3 器件照片以及测试结果。(a)SPAD 显微照片;(b) I-V 直流特性曲线

Fig. 3 Device photos and test results. (a) Micrograph of the SPAD; (b) I-V DC characteristic curves

3.2 DCR 与后脉冲

在无光环境下 SPAD 因内部缺陷产生电子-空穴对,从而导致雪崩现象即暗计数的发生。使用 FPGA 测试板和示波器统计每秒内 SPAD 器件的雪崩脉冲个数,得到 DCR。图 4(a)所示为新型 SPAD 器件在 25~80 $^{\circ}\text{C}$ 下的 DCR 变化曲线。当 $V_{\text{ex}}=5 \text{ V}$ 时,室温下的 DCR 仅为 $0.56 \text{ s}^{-1} \cdot \mu\text{m}^{-2}$;当 $V_{\text{ex}}=2\sim 5 \text{ V}$ 时,DCR 缓慢升高。随着温度从 25 $^{\circ}\text{C}$ 上升至 80 $^{\circ}\text{C}$,DCR 增加了约 2 个数量级。由于 DCR 表现出强烈的温度依赖性,测量了 SPAD 器件在 1~5 V 下的激活能,如图 4(a)插图所示。当温度低于 40 $^{\circ}\text{C}$ 时,激

活能(E_a)小于 0.16 eV,表明隧穿效应是 DCR 的重要影响因素。随着 V_{ex} 的增加,激活能逐渐降低,隧穿效应的影响变得更加显著。在超过 40 $^{\circ}\text{C}$ 的高温下, E_a 增加到约 0.62 eV,超过 Si 带隙的一半,表明热激发效应成为 DCR 的重要影响因素^[9]。SPAD 器件的后脉冲概率(AP)可以通过暗计数脉冲间到达时间的直方图表征,图 4(b)所示为后脉冲测量结果。当淬灭电阻为 100 k Ω 时,死区时间约为 14 μs ,记录大量暗计数并对计数分布进行拟合。在 5 V 偏置电压下,该器件的 AP 为 1.2%,表明器件雪崩倍增区的缺陷浓度较低^[10]。

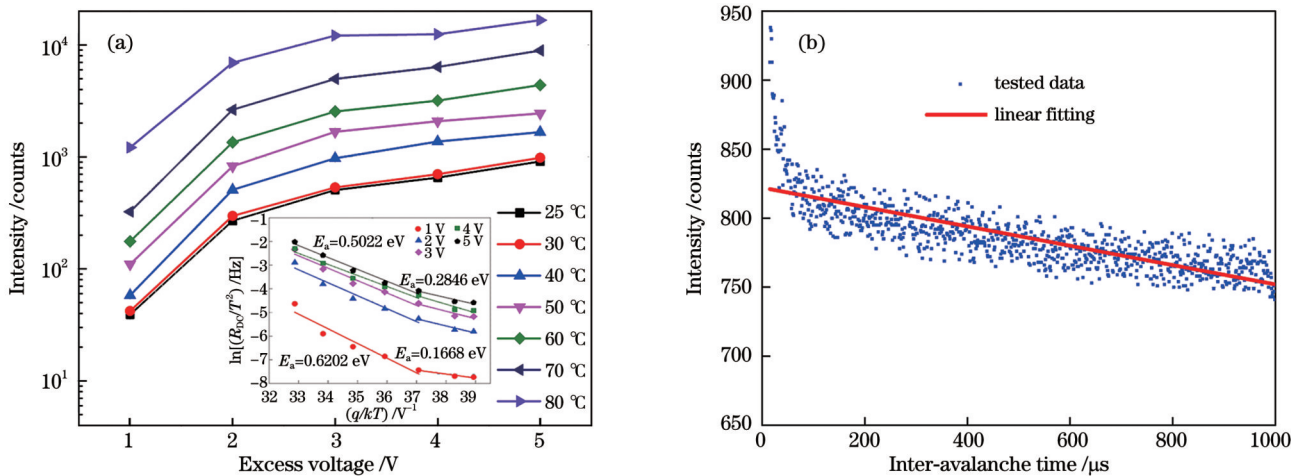


图 4 DCR 与 AP 测试结果。(a)不同温度下 DCR 随过偏压的变化;(b) $D_3=5 \mu\text{m}$ 时的后脉冲直方图统计

Fig. 4 Test results of DCR and AP. (a) DCR versus excess voltage at different temperatures; (b) post-pulse histogram when $D_3=5 \mu\text{m}$

3.3 PDP

PDP 测量设备包括波长范围为 405~940 nm 的激光器、积分球、光功率计和 FPGA 测试板。将 SPAD 器件放置在积分球的一个端口,并将不同波长的单色激光通过光纤耦合到积分球中,使用光功率计测量激光功率。为了防止光子堆叠效应,激光功率设置为 10 nW。PDP(P_{PD})的计算公式为

$$P_{PD} = \frac{N - R_{DC}}{N_{\lambda}}, \quad (1)$$

式中: N_{λ} 为某一波长下到达器件感光区的光子数; N 为实测的光子雪崩脉冲数; R_{DC} 为器件的 DCR。PDP 的测试结果如图 5 所示,随着 V_{ex} 增加,雪崩触发概率增大,PDP 增大。当 $V_{ex}=5$ V 时,SPAD 器件的 PDP 峰值在 600 nm 附近,达到 41.5%;随着光子波长的增加,PDP 明显降低,这是因为光子的吸收系数随着波长的增加而显著降低^[11]。由于该 SPAD 器件具有深结的宽雪崩倍增区,这有利于近红外光子吸收而触发雪崩效应^[12-13],因此近红外波段 901 nm 处的 PDP 达到 6%,在宽光谱范围内获得较高的响应度。图 6 展示了

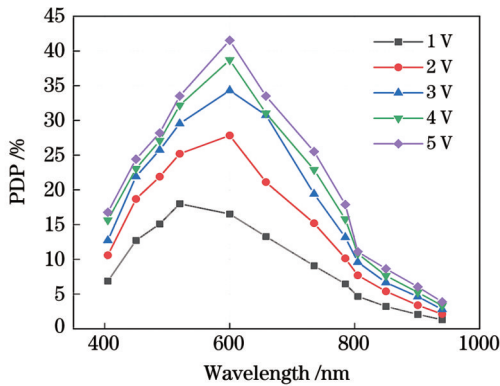


图 5 PDP 对光子波长响应曲线

Fig. 5 PDP as a function of photon wavelength

表 1 P-I-N 结构 SPAD 关键性能对比

Table 1 Key performance comparison of P-I-N SPADs

Method	Technology	Junction	AP / %	V_{BD} / V	Peak PDP / % @ λ / nm	PDP / % @901 nm	DCR / (s ⁻¹ · μ m ⁻²) @ V_{EX} / V
Gramuglia <i>et al.</i> ^[2]	180 nm CMOS	P-I-N	0.12-3	22	55@480	4.6	0.2@6
Liu <i>et al.</i> ^[3]	55 nm CMOS	P ⁺ /DNW	N/A	26.1	20.3@660	5.9	20@2
Sun <i>et al.</i> ^[4]	55 nm BSI CMOS	P ⁺ /N well	N/A	20.5	25.2@640	12	0.36@2.5
Wu <i>et al.</i> ^[5]	180 nm CMOS	N ⁺ /P well	4.5	30.8	26@520	3.2	4.03@10
Veerappan <i>et al.</i> ^[6]	180 nm CMOS	P-I-N	0.08	<40	47	5	1.5@11
Vornicu <i>et al.</i> ^[7]	110 nm CIS	PW/DNW	0.5	N/A	64@500	5.5	0.4@3
Gramuglia <i>et al.</i> ^[8]	55 nm BCD	DPW/BNW	0.97	31.5	62@530	5.6	0.1-2.6@1-7
This work	180 nm BCD	P-I-N	1.2	56	41@600	6	0.56@5

5 总 结

采用 180 nm BCD 工艺制备了一种工作在盖革模

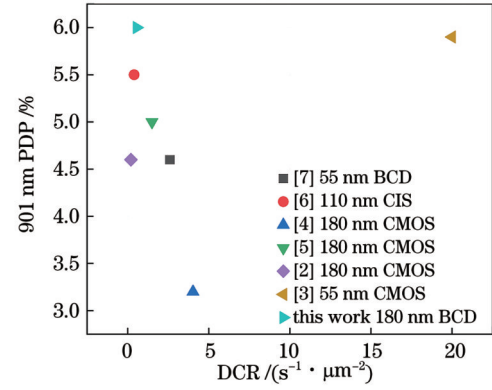


图 6 所设计 SPAD 与其他性能先进的 SPAD 器件的比较

Fig. 6 Comparison of proposed SPAD with the other state-of-the-art SPADs

所设计的 SPAD 与国际上先进器件在 901 nm 处的 PDP 的对比,可以看出,其在近红外波段的 PDP 和暗计数性能方面具有极大的优势。

4 与国际先进成果的对 比

表 1 总结了已报道的几种最先进 SPAD 器件的性能指标。文献[2]和[6]提出的器件均为 P-I-N 结构,但缺少额外的 P 型注入层,其近红外波段的 PDP 小于 5.6%。文献[3]采用浅结的 P⁺/DNW 结构,虽然使用先进的 55 nm 工艺制程,但峰值 PDP 较低,而且 DCR 很高。基于 110 nm CIS 工艺的 PW/DNW 结构获得了高的峰值 PDP,但近红外波段的 PDP 只有 5.5%。采用先进制程的背照式 SPAD 器件^[4,8]大幅提升了近红外波段的 PDP,但制造成本高昂。相比之下,所提出的 P 型注入增强型 P-I-N 结构器件采用低成本 BCD 工艺,不需要改变任何工艺参数,即可实现较高的峰值 PDP 和近红外 PDP,而且 DCR 和后脉冲率也较低。

式下的 P 型注入增强型 P-I-N 结构的 SPAD。该器件的深雪崩倍增区位于 P 型漂移层和高压 N⁺埋层之间,更宽和更深的雪崩倍增区提高了近红外波段的

PDP,而双保护环的设计降低了雪崩区电场强度,避免了边缘击穿,优化了暗计数噪声。通过额外的P型注入层还有效降低了器件的雪崩电压。测试结果表明,SPAD在400~800 nm的宽光谱范围内实现了10%以上的PDP,并且在5 V过偏压下600 nm处峰值PDP高达41%,901 nm处PDP大于6%,DCR小于 $0.56 \text{ s}^{-1} \cdot \mu\text{m}^{-2}$,后脉冲率仅为1.2%,表现出优异的电学和光学性能。

参 考 文 献

- [1] 张维宇, 汪洋, 金湘亮. 双波峰响应CMOS单光子探测器的设计与优化[J]. 光学学报, 2021, 41(17): 1704001.
Zhang W Y, Wang Y, Jin X L. Design and optimization of double-wave-peak response CMOS single-photon detector[J]. Acta Optica Sinica, 2021, 41(17): 1704001.
- [2] Gramuglia F, Wu M L, Bruschini C, et al. A low-noise CMOS SPAD pixel with 12.1 ps SPTR and 3 ns dead time[J]. IEEE Journal of Selected Topics in Quantum Electronics, 2022, 28(2): 3800809.
- [3] Liu Y, Liu M L, Ma R, et al. A wide spectral response single photon avalanche diode for backside-illumination in 55-nm CMOS process[J]. IEEE Transactions on Electron Devices, 2022, 69(9): 5041-5047.
- [4] Sun W B, Wang Y X, Liu M L, et al. A back-illuminated $4 \mu\text{m}$ P^+ N-well single photon avalanche diode pixel array with $0.36 \text{ Hz}/\mu\text{m}^2$ dark count rate at 2.5 V excess bias voltage[J]. IEEE Electron Device Letters, 2022, 43(9): 1519-1522.
- [5] Wu J Y, Liu C H. Design and characterization of n/p-well CMOS SPAD with low dark count rate and high photon detection efficiency[J]. IEEE Transactions on Electron Devices, 2023, 70(2): 582-587.
- [6] Veerappan C, Charbon E. A low dark count P-I-N diode based SPAD in CMOS technology[J]. IEEE Transactions on Electron Devices, 2016, 63(1): 65-71.
- [7] Vornicu I, López-Martínez J M, Bandi F N, et al. Design of high-efficiency SPADs for LiDAR applications in 110 nm CIS technology[J]. IEEE Sensors Journal, 2021, 21(4): 4776-4785.
- [8] Gramuglia F, Keshavarzian P, Kizilkan E, et al. Engineering breakdown probability profile for PDP and DCR optimization in a SPAD fabricated in a standard 55 nm BCD process[J]. IEEE Journal of Selected Topics in Quantum Electronics, 2022, 28(2): 3802410.
- [9] Sicre M, Federspiel X, Mamdy B, et al. Characterization and modeling of DCR and DCR drift variability in SPADs[C]//2023 IEEE International Reliability Physics Symposium (IRPS), March 26-30, 2023, Monterey, CA, USA. New York: IEEE Press, 2023.
- [10] Sun F Y, Xu Y, Wu Z, et al. A simple analytic modeling method for SPAD timing jitter prediction[J]. IEEE Journal of the Electron Devices Society, 2019, 7: 261-267.
- [11] Deng S J, Li X, Chen M, et al. Design and analysis of an afterpulsing auto-correction system for single photon avalanche diodes[J]. IEEE Photonics Technology Letters, 2021, 33(6): 293-296.
- [12] 康岩, 薛瑞凯, 李力飞, 等. 基于SPAD的共光路扫描三维成像阵列学报[J]. 激光与光电子学进展, 2021, 58(10): 1011024.
Kang Y, Xue R K, Li L F, et al. Coaxial scanning three-dimensional imaging based on SPAD array[J]. Laser & Optoelectronics Progress, 2021, 58(10): 1011024.
- [13] 付爽, 田小芮, 杨杰, 等. 基于单光子阵列相机的激光测速[J]. 激光与光电子学进展, 2023, 60(8): 0811023.
Fu S, Tian X R, Yang J, et al. Laser velocimetry based on single-photon array camera[J]. Laser & Optoelectronics Progress, 2023, 60(8): 0811023.

A P-I-N Structure Single-Photon Avalanche Diode Detector with Low Dark Count Rate

Li Zheng¹, Liu Danlu¹, Dong Jie¹, Bian Dajing¹, Xu Yue^{1,2*}

¹College of Integrated Circuit Science and Engineering, Nanjing University of Posts and Telecommunications, Nanjing 210023, Jiangsu, China;

²National and Local Joint Engineering Laboratory of RF Integration & Micro-Assembly Technology, Nanjing 210023, Jiangsu, China

Abstract

Objective Over the past few decades, single-photon detection technology has rapidly developed. Single-photon avalanche diode (SPAD) detectors operating in Geiger mode have advantages such as high sensitivity, fast response speed, and strong capability for single-photon detection. As a result, they have been widely used in optical sensing fields such as quantum communication, lidar, and fluorescence lifetime imaging. SPAD arrays compatible with CMOS technology have gained significant attention due to their high integration and miniaturization. In laser radar applications, SPADs are employed to receive returning photons. However, optical signals are susceptible to environmental factors like dust and weather conditions. The received light intensity might be at the single-photon level, and high dark count noise can degrade device performance. Considering the potential harm of short-wavelength lasers to human eyes, the design of SPAD devices with low dark counts and high photon detection probabilities has become a hot research direction.

Methods The SPAD (Fig. 1) employs a P-I-N diode structure, with the avalanche region located between the P-type drift region and the high-voltage N^+ buried layer. The P epitaxial layer serves as the intrinsic region, with P-trap guard rings and virtual guard rings surrounding the P-doped region to mitigate the impact of shallow trench isolation on dark count rates (DCR). The proposed SPAD devices with GRW of 3, 4, 5 μm are simulated based on 0.18 μm BCD technology to study the impact of GRW on device performance [Fig. 2(a)]. Simulation results show that the device can only work normally at GRW of 5 μm without a large edge electric field, and it will also cause the dark count to decrease. Figure 2(c) illustrates the 2D electric field distributions when STI extends into PW. Changing STI appropriately can hardly improve the electric field strength.

Results and Discussions The I - V characteristic of the SPAD is firstly measured which exhibits avalanche breakdown voltage at around 56 V [Fig. 3(c)], showing no difference to the TCAD simulation results (Fig. 2). DCR measurement results [Fig. 4(a)] show that the variation of DCR with V_{ex} is not obvious and this value is more dependent on temperature changes. The data demonstrates excellent performance of $0.56 \text{ s}^{-1} \cdot \mu\text{m}^{-2}$ at 23 $^{\circ}\text{C}$ and 5 V excess bias voltage. The PDP measurements (Fig. 5) show that the peak PDP reaches 41.5% (600 nm) at $V_{\text{ex}}=5 \text{ V}$. Moreover, due to the wide depletion layer, there is a higher response sensitivity for near-infrared photons (780–940 nm) and PDP at 905 nm is more than 6%.

Conclusions We propose an additional P-type injection enhanced P-I-N structure SPAD based on the SMIC 180 nm BCD process. The test results show that at $V_{\text{ex}}=5 \text{ V}$, the PDP peak of the SPAD reaches 41.5%, and the near-infrared PDP at the 905 nm wavelength is larger than 6%. At room temperature, it achieves a median DCR of $0.56 \text{ s}^{-1} \cdot \mu\text{m}^{-2}$ and a very low afterpulsing probability $<1.2\%$ when quenched passively with a dead time of 14 μs .

Key words detectors; single-photon avalanche diode (SPAD); P-I-N structure; photon detection probability (PDP); dark count rate (DCR)